

Probabilistic Fault Displacement Hazard Analysis for North Tabriz Fault

Mohammadreza Hosseyni¹, Habib Rahimi,²

1. M.Sc. Graduated, Department of Earth Physics, Institute of Geophysics, University of Tehran, Tehran, Iran

2. Associate Professor, Department of Earth Physics, Institute of Geophysics, University of Tehran, Tehran, Iran

Corresponding author: Habib Rahimi; email: rahimih@ut.ac.ir

Abstract:

The probabilistic fault displacement hazard analysis is one of the new methods of estimating the amount of possible displacement in the area at the hazard of causal fault rupture. In this study, using the probabilistic approach and earthquake method introduced by Youngs et al., 2003, the surface displacement of the North Tabriz fault has been investigated, and the possible displacement in different scenarios has been estimated. By considering the strike-slip mechanism of the North Tabriz fault and using the earthquake method, the probability of displacement due to surface ruptures caused by the 1721 and 1780 North Tabriz fault earthquakes has been explored. These events were associated with 50 and 60 km of surface rupture, respectively. The 50-60 km long section of the North Tabriz fault was selected as the source of possible surface rupture.

We considered two scenarios according to possible displacements, return periods, and magnitudes which are reported in paleoseismic studies of the North Tabriz fault. In the first scenario, possible displacement, return period, and magnitude was selected between zero to 4.5; 645 years and $M_w \sim 7.7$, respectively. In the second scenario, possible displacement, return period and magnitude were selected between zero to 7.1, 300 years, and $M_w \sim 7.3$, respectively. For both mentioned scenarios, the probabilistic displacements for the rate of exceedance 5% in 50, 475, and 2475 years for the principle possible displacements (on fault) of the North Tabriz fault have been estimated. For the first and second scenarios, the maximum probabilistic displacement of the North Tabriz fault at a rate of 5% in 50 years is estimated to be 186 and 230 cm. Also, mentioned displacements for 5% exceedance in 475 years and 2475 years in both return periods of 645 and 300 years, are estimated at 469 and 655cm.

Keywords: Surface rupture, Hazard, probabilistic fault displacement, North Tabriz fault, Iran.

1- Introduction

Earthquakes, not only because of earth-shaking but also because of surface ruptures, are a serious threat to many human activities. Reducing earthquake losses and damages requires predicting the amplitude and location of ground movements and possible surface displacements in the future. Fault displacement hazard assessments are based on empirical relationships obtained using historical seismic rupture data. These relationships evaluate the probability of co-seismic surface slip of ruptures on fault (primary) and outside the fault (distributed) for different magnitudes

and distances to the causal fault. In addition, these relationships make it possible to predict the extent of fault slip on or near the active fault (Stephanie Baiz et al., 2019).

A way to reduce the effects of fault rupture hazards on a structure is to develop the probability of fault displacement. This approach can be taken into account the rate of exceedance of different displacement levels of the event under a structure, along with a displacement hazard curve (Youngs et al., 2003). So far, fault displacement data have been collected and analyzed by several researchers to evaluate the fault rupture properties. Investigation of fault displacement and extraction of experimental relationships are reported by Wells and Coppersmith (1993 and 1994) and reviewed by Petersen and Wesnousky (1994). To be considered, each earthquake causes a superficial shaking at the site, but each earthquake does not cause a surface rupture in the area. Therefore, only the data of earthquakes that have caused the rupture in the region are used to obtain the attenuation relationships (Youngs et al., 2003).

A method for estimating the probabilistic fault displacement hazard for strike-slip faults in the world has been presented, mapped due to the impact of fault displacement hazard on the fault trace type and the complexity of this effect and hazard of fault displacement for strike-slip faults studied (Petersen et al., 2011). Principal displacements are considered primary ruptures that occur on or within a few meters of the active fault. Distributed displacements outside the fault are causative and usually appear as discontinuous ruptures or shears distance several meters to several hundred kilometers from the fault trace. The principal and distributed displacements are introduced as net displacements derived from horizontal and vertical displacements (Petersen et al., 2011).

To estimate the probabilistic fault displacement hazard, we used the Petersen et al., 2011 method, but newly some studies have been conducted in this approach. Recently, Katona (2020) investigated the hazard of surface displacement due to faults in the design of nuclear power plants. Nurminen et al. (2020) concentrate on off-fault rupturing and developed an original probability model for the occurrence of distributed ruptures using 15 historical crustal earthquakes. Goda (2021) proposed an alternative approach based on stochastic source modeling and fault displacement analysis using Okada equations. The developed method is applied to the 1999 Hector Mine earthquake.

In this study, based on the results of a paleoseismic study reported by Hesami et al. (2003) on the North Tabriz fault, the section with a length of 50 - 60 km was considered a source of possible rupture in the future. To describe the possible behavior of the displacement rupture hazard of the North Tabriz fault, sites at distances of 50 m from each other and cells with dimensions of $25 \times 25 \text{ m}^2$ on fault trace were considered, which is shown in Figure 1. Also, according to the study by Petersen et al. (2011), the trace of the North Tabriz fault was considered a simple trace due to the absence of large instrumental earthquakes that are associated with surface rupture. Many studies have been done on the historical displacements of the North Tabriz fault. According to the results of paleoseismic studies reported by Hesami et al. (2003) and Ghasemi et al. (2015), the probabilistic displacement is between zero to 4.5 and zero to 7.1 m, respectively. The magnitude and return period of large earthquakes are considered 645 years with $M_w \sim 7.7$ and 300 years with $M_w \sim 7.3$ according to Mousavi et al. 2014 and Dejamour et al., 2011, respectively.

In the first step, probabilistic fault displacement and the annual rate of exceedance of displacement for two given scenarios (645 years with $M_w \sim 7.7$) and (300 years with $M_w \sim 7.3$) have been achieved by considering 5% in 50, 475,

and 2475 years at the site with geographical coordinates (38.096, 46.349). In the second step, due to the passage of the North Tabriz Fault through the city of Tabriz, considering a 2 km long section from the North Tabriz Fault, the probabilistic displacement has been estimated, and the probabilistic displacement 2D map is explored.

72

732- Seismotectonic

With over two million people and an area of 167 square kilometers in northwestern Iran, Tabriz is one of the most populated cities in the country that has experienced devastating earthquakes throughout history. One of the main problems of Tabriz City is the proximity of the city to the North Tabriz fault and the expansion of constructions around it. Based on the reported historical earthquakes by Berberian and Arshadi (1979), since 858 AD., this city and the surrounding area have experienced several large and medium destructive earthquakes.

The focal mechanism of earthquakes in northwestern Iran and southeastern Turkey shows that the convergence between the Saudi and Eurasian plates becomes appreciable during right-lateral strike-slip faults. The strike-slip fault is the southeastern continuation of the North Anatolian Fault into Iran, consisting of discontinuous fault sections with a northwest-southeast extension (Jackson and Mackenzie et al., 1992). Some of these fault fragments have been ruptured and left deformed along with the earthquakes in 1930, 1966, and 1976 (Hesami et al., 2003).

Nevertheless, the North Tabriz fault is one of the components of this right-lateral strike-slip system, which has not had a major earthquake during the last two centuries. Among the many historical earthquakes in the Tabriz region, only three devastating earthquakes with a magnitude of $M_s \sim 7.3$ in 1042, 1721, and 1780 with a magnitude of $M_s \sim 7.4$ had been associated with a surface rupture along the North Tabriz fault (Hesami et al., 2003). The 1721 and 1780 AD earthquakes were along with at least 50 and 60 km of surface rupture (about 40 km overlap), respectively. Berberian et al., 1997 believe that large earthquakes along the North Tabriz fault are concentrated at specific times and spatially related.

The occurrence of the 1976 Chaldoran earthquake in Turkey, which was accompanied by about 55 km of fractures, indicates that the length of the surface fracture caused by historical earthquakes in this region probably varies from about 50 to 60 km (Toxos et al., 1977). A more detailed study of the temporal distribution of earthquakes in Tabriz by Berberian and Yates (1999) also shows the cluster distribution of earthquakes over time. Due to the absence of seismic events for more than 200 years in the Tabriz area (decluttering period), the study area has passed the final stages of stress storage, and it is ready to release the stored energy. Therefore, Hesami et al., 2003 investigated the Spatial-temporal concentration of earthquakes associated with the North Tabriz fault. Based on paleontological seismic studies on the western part of the North Tabriz fault, Hesami et al., 2003 introduced four earthquakes that occurred continuously on the western part of the North Tabriz fault. The return periods of these earthquakes were suggested to be 821 ± 176 years. The amount of right-lateral strike-slip displacement, during each seismic event, of the North Tabriz fault, has been estimated at 3.5 to 4.5 m. In addition, Berberian et al., 1997 considered the possibility of fracturing all parts of the North Tabriz fault at once and mentioned it as one of the critical issues in the earthquake hazard for the Tabriz city and the northwestern region of Iran.

1043- Methodology of probabilistic fault displacement hazard analysis

105 In this study, the method introduced by Petersen et al., 2011 has been used to estimate the probabilistic fault
106 displacement hazard caused by the North Tabriz fault. Details of the mentioned method are provided in Petersen et
107 al., 2011, and a summary of this approach is provided here.

108 Probabilistic seismic hazard analysis has been used since its development in the late 1960s and early 1970s
109 to assess shaking hazards and to establish seismic design parameters (Cornell, 1968 and 1971). A method for analyzing
110 the hazard of probabilistic fault displacement was introduced in two approaches of earthquake and displacement
111 (Youngs et al., 2003). This method was first proposed to estimate the displacement of Yucca Mountain faults, which
112 were the landfill of nuclear waste (Stepp et al., 2001). Then, the probabilistic fault displacement hazard analysis
113 method was introduced for an environment with normal faults, and the probability distributions obtained for each type
114 of fault in the world can be used in areas with similar tectonics (Youngs et al., 2003).

115 The earthquake approach is similar to the analysis of probabilistic seismic hazards related to displacement, features
116 such as faults, partial shear, fracture, or unbroken ground at or near the ground surface so that the attenuation
117 relationships of the fault displacement replace the ground shaking relationships. In the displacement approach, without
118 examining the rupture mechanism, the displacement characteristics of the fault observed at the site are used to
119 determine the hazard in that area.

120 The exceedance rate of displacements and the distribution of fault displacements are obtained directly from the fault
121 characteristics of geological features (Youngs et al., 2003). To calculate the rate of exceedance in the earthquake
122 approach, similar to probabilistic seismic hazard analysis relationships were used. The rate of exceedance, $v_k(z)$, is
123 calculated according to the Cornell relationship (1968 and 1971) as follows (Youngs et al., 2003):

$$v_k(z) = \sum_n \alpha_n(m^0) \int_{m^0}^{m_n^u} f_n(m) \left[\int_0^\infty f_{kn}(r|m) \cdot P^*(Z > z|m, r) \cdot dr \right] \cdot dm \quad (1)$$

125 In which the ground motion parameter, (Z), (maximum ground acceleration, maximum response spectral acceleration)
126 exceeds the specified level (z) at the site (k). Considering Equation (1) and calculating the exceedance rate of
127 displacement (D) from a specific value (d), the displacement parameter replaces the parameters of ground motion
128 (Youngs et al., 2003):

$$v_k(d) = \sum_n \alpha_n(m^0) \int_{m^0}^{m_n^u} f_n(m) \left[\int_0^\infty f_{kn}(r|m) \cdot P^*(D > d|m, r) \cdot dr \right] \cdot dm \quad (2)$$

129 The expression $P(D > d|m, r)$ is the "attenuation function" of the fault displacement at or near the earth's surface. This
130 displacement attenuation function is different from the usual ground motion attenuation function and includes the
131 multiplication of the following two probabilities (Youngs et al., 2003):

$$P_{kn}^*(D > d|m, r) = P_{kn}(\text{Slip}|m, r) \cdot P_{kn}(D > d|m, r, \text{slip}) \quad (3)$$

132 Which D and d are the Displacements on fault (principal fault) and displacement on the outside of the fault (distributed
133 fault), respectively (x, y) are considered as coordinates of the site. r, z^2, I, L , and s are the vertical distance from the

fault, area, the distance of site on fault rupture to the nearest rupture, the total length of the fault surface rupture, and the rupture distance to the end of the fault, respectively. The definition of these variables is shown in figure (2). The following Equation has been used to obtain the exceedance rate of probabilistic displacement due to the principal fault (on fault) (Petersen et al., 2011):

$$\lambda(D \geq D_0)_{xyz} = \quad (4)$$

$$\alpha(m) \int_{m,s} f_{M,s}(m, s) P[sr \neq 0|m] * \int_r P[D \neq 0|z, sr \neq 0] * P[D \geq D_0 | l/L, m, D \neq 0] f_R(r) dr dm ds$$

The magnitude of the earthquake is indicated by m. In relation 4 and to assess the displacement hazard due to fault rupture, the probability density functions that describe displacement potential due to earthquakes on or near a rupture, as well as the probabilities that the potential for non-zero ruptures are used (Petersen et al., 2011). In the following, each of the parameters for estimation of probabilistic fault displacement hazard is described.

3-1 Probability density function

The probability density function $f_{M,s}(m, s)$ determines the magnitude of the earthquake and the location of the ruptures on a fault. Since the magnitude and the rupture position on the causal fault are correlated, a probabilistic distribution is used to calculate these parameters. In the next step, the variability in the rupture location is considered. A probability density function $f_R(r)$ is considered to define the area of perpendicular distances (r) to the site to different potential ruptures (Petersen et al., 2011).

3-2 Probabilities

Probability $P[SR \neq 0 | M]$ is the ratio of cells with rupture on the principal fault to the total number of cells considered. Therefore, the probability of surface rupture $P[SR \neq 0 | M]$ is considered due to a certain magnitude M due to faulting. According to studies by Wells and Coppersmith (1993), due to the formulation of empirical relationships between different fault parameters, probability has been obtained for different faults in the world, such as strike-slip, normal, and revers. Therefore, in hazard analysis of fault displacement, it is necessary to investigate the possibility of surface rupture with magnitude (M) on the ground so as a result, the equation (5) introduced by Wells and Coppersmith (1993) can be used. According to this relation, the coefficients a and b are constant, and strike-slip faults with -12.51 and 2.553 have been reported. This relationship has a 10% probability for the size of Mw~5 and a 95% probability of surface rupture for a magnitude of Mw~7.5 ((Rizzo et al., 2011).

$$P[sr \neq 0|m] = \frac{e^{a+bm}}{1+e^{a+bm}} \quad (5)$$

This rupture probability was used to estimate the exceedance rate of displacement because of earthquakes such as Loma-Prieta in 1989 with a magnitude of Mw~6.9 and Alaska in 2002 with a magnitude of Mw~6.7. These earthquakes did not cause rupture to reach the earth's surface. Therefore, these two earthquakes did not cause surface

deformation and are considered non-tectonic phenomena (Petersen et al., 2011). The expression $P[D \neq 0|z, sr \neq 0]$ indicates the probability of non-zero displacement at a distance r from the rupture in an area of size z^2 and due to the magnitude event m associated with the surface rupture. The probability $P[D \geq D_0 | l/L, m, D \neq 0]$ for displacements more significant than or equal to the value given at this site is intended for the principal displacement (on fault). This probability is obtained by integrating around a log-normal distribution (Petersen et al., 2011).

3-3 Rate parameter $\alpha(m)$:

When the potential magnitude of an earthquake a certain magnitude is modeled, it is possible to estimate how often these ruptures occur. The, $\alpha(m)$, rate parameter used describes the frequency of repetition of these earthquakes in this model. This parameter is a function of magnitude and can only function as a single rupture function or a function of cumulative earthquakes above the magnitude of the minimum importance in engineering projects (Youngs et al., 2003). This parameter is usually based on slip rate, paleoseismic rate of large earthquakes, or historical fault rate earthquakes and is described in earthquake units per year. By removing the $\alpha(m)$ parameter from Equation (4), the Deterministic Fault Displacement Hazard can be estimated (Petersen et al., 2011).

3-4 Cell size:

In calculating the hazard of principal fault displacements, as shown in Eq. (4), by changing the size of the cells, the level of hazard will not change and this parameter can be examined by the availability of principal displacement data in the study area. In calculating the hazard of distributed rupture (distributed displacement), considering the method of Youngs et al. (2003), by modeling secondary displacements up to a distance of 12 km from the fault, the probability of surface rupture was investigated. According to studies by Petersen (2011), the relationship between the calculations of the probability of rupture of the principal faults (5), in calculating the probability of rupture of the distributed faults became the following relationship (Petersen et al., 2011):

$$\ln(p) = a(z) \ln(r) + b(z) \quad (6)$$

The values of the coefficients used for the cell sizes of 25×25 to $200 \times 200 \text{ m}^2$ in the above relationship are given in Table 1 (Petersen et al., 2011).

3-5 Surveying accuracy

The accuracy of fault location is a function of geological and geomorphic conditions that play an essential role in diagnosing and interpreting a geologist in converting this spatial information into geological maps and fault geographic information systems. A fault map is generated using aerial photography imagery, interpretation of fault patterns from geomorphology, and conversion of fault locations into a base map. In many cases, identifying the location and trace of the fault may be difficult because sediments and erosion may obscure or cover the fault surface, leading to more uncertainty in identifying the actual location of the fault. Therefore, trace mapped faults are divided into four categories: accurate, approximate, inferred, and concealed, based on how clearly and precisely they are located (Petersen et al., 2011).

A practical example shows that an active fault with large earthquakes repeated over several hundred years, fault rupture hazard analysis should be one of the critical topics considered for the design of structures or pipelines that are close to this fault, and if the fault has a complex or straightforward trace, avoiding the fault from the constructor to a distance of 150 and 300 meters, respectively. Table 2 summarizes the standard deviations for the displacements observed in strike-slip earthquakes for different classifications of mapping accuracy (Petersen et al., 2011). According to the exponential values obtained from these fitting equations, the mean displacement will be obtained. The following Equation has been used to obtain the mean displacement (Petersen et al., 2011):

$$D_{mean} = e^{\mu + \sigma^2/2} \quad (7)$$

3-6 Epistemic and Aleatory uncertainty

There are uncertainties about the quality of mapping and the complexity of the fault trace that lead to epistemic uncertainty at the site of future faults. The probability density function for r includes both epistemic and aleatory components. Displacements on and off the principal fault can include components of epistemic uncertainty and random variability. Epistemic uncertainty is related to displacement measurement errors along fault rupture. Random variability is related to the natural variability in fault displacements between earthquakes. However, the measured variability in ruptures involves epistemic mapping uncertainties because there is currently no data to separate these uncertainties. In addition, epistemic uncertainty of location is introduced due to limitations in the accuracy of basic maps or images and the accuracy of the equipment used to transfer this information to the map or database (Petersen et al., 2011).

3-7 Attenuation relationship of strike-slip faults

In this study, to estimate the probabilistic displacement of the North Tabriz fault, the attenuation relationship of Petersen et al. (2011) has been used. The rupture displacement data obtained from the principal fault are scattered but are generally the most scattered near the fault rupture center and decrease rapidly at the end of the rupture. In some earthquakes, including the Borgo Mountain earthquake in 1968, the most significant displacement was observed near the end of the fault surface rupture (Petersen et al., 2011). Many of the collected surface rupture data behave asymmetrically ruptured (Wesnousky et al., 2008). However, there is currently no way to determine surface rupture areas that have larger displacements. Thus, the distribution of asymmetric displacements along the length of a fault will define more considerable uncertainties, especially near the end of the fault rupture (Petersen et al., 2011). To determine the displacement distribution, and the principal fault, two different approaches were introduced by Petersen et al. (2011). In the first approach, the best-fit equations using the least-squares method related to the natural logarithm of the displacement ratio of magnitude and distance were developed in a multivariate analysis (Paul Rizzo et al., 2013). In the second approach, the displacement data is normalized by the average displacement as a distance function. In normalized analysis, magnitude is not directly considered but influences calculations through the presence of magnitude in the mean displacement, which is calculated through the studies of Wells and Coppersmith (1994). Three

models (bilinear, elliptical and quadratic) were considered to provide the principal fault displacement in multivariate and normalized analysis (Petersen et al., 2011). However, in multivariate analysis, the three introduced models have the same aleatory uncertainty, and there is no clear basis for preferring one model to the other models. As a result, in the probabilistic displacement hazard analysis, all three models with the same weights were used according to Table 3. The results obtained from the multivariate analysis were preferred over the normalized analysis because, in the normalized analysis, the stochastic uncertainty of calculating the mean displacement from the Wells and Coppersmith (1994) study is added to the stochastic uncertainty of the results of the Petersen attenuation relationships (Paul Rizzo et al., 2013).

In this study, multivariate analysis and probabilistic displacement estimation have been used in the three mentioned models. The Equation of the three models is obtained in the multivariate method as shown in Table 3, and 5% uncertainty was considered in the modeling of the strike-slip displacement data (Petersen et al., 2011):

4 Results and Discussions

In this study, we assumed the North Tabriz fault as a simple trace with the strike-slip focal mechanism. Due to the lack of instrumental data on surface ruptures, two scenarios ($M_w \sim 7.7$, 645years), and ($M_w \sim 7.3$, 300years) was considered a probabilistic surface rupture in the future. The length of the fault section was considered 50- 60 km and the probabilistic displacement, and the annual exceedance rate was estimated by considering one of the sites located on the Tabriz fault trace related to the total segment as shown in Figure 1. In addition, for each scenario, two values of displacement (zero to 4.5m) and (zero to 7.1m) were considered according to Hessami et al., 2003 and Ghassemi et al., 2015, respectively. Furthermore, considering the reported method by Petersen et al., 2011, the probabilistic displacements for an exceedance rate of 5% in 50, 475, and 2475 years for the principal probabilistic displacements (on fault) of the North Tabriz fault have been explored. The obtained results in this study can be summarized as follows.

By considering the reported 4.5 m probable surface displacement by Hessami et al., 2003, maximum displacement for the first scenario ($M_w \sim 7.7$, 645years) and 5% in 50, 475, and 2475years were estimated at 186, 469, and 469 cm. For the second scenario ($M_w \sim 7.3$, 300years), the maximum displacement was calculated at 230, 469, and 469cm, respectively as shown in figure (3a). In addition, by considering the 7.1m probable surface displacement reported by Ghassemi et al., 2015, maximum displacement for the first scenario of ($M_w \sim 7.7$, 645years) and 5% in 50, 475, and 2475years was estimated at 186, 655, and 655cm. For the second scenario ($M_w \sim 7.3$, 300years), the maximum displacement was calculated at 230, 655, and 655 cm, respectively which is shown in figure (3b).

According to the results shown in Figures 3a and 3b, although in some cases and distances, the estimated maximum displacement values are the same, at farther distances perpendicular to the site, these values are different from each other.

For both scenarios ($M_w \sim 7.7$, 645 years and $M_w \sim 7.3$, 300 years), taking into account the maximum possible displacements reported from other studies (0 to 4.5m and 7.1m), the maximum displacements for 5% in 475 years were observed up to a distance of 60 meters perpendicular to the assumed site.

For the first scenario ($M_w \sim 7.7$, 645 years), the maximum displacement for 5% in 2475 years using probable displacements 0 to 4.5m and 0 to 7.1 m were calculated up to 100m and 80m perpendicular to the assumed site, respectively. For the second scenario ($M_w \sim 7.3$, 300 years), the maximum displacement for 5% in 2475 years using probable displacement of 0 to 4.5m and 0 to 7.1 m were observed up to 80m and 40m perpendicular to the assumed site, respectively.

As mentioned, the fitting models (bilinear, elliptical, and quadratic) have similar uncertainties, and in this section, we compared the estimated displacements obtained by using these models. In this study, the bilinear model is used to obtain probabilistic displacements. The values of the probabilistic displacements were obtained for the mentioned models. In figure 4, estimated probability displacement has been compared using different fitting models.

In the next step, for both scenarios of 4.5 and 7.1m displacements, the annual rate of exceedance of displacement (5% in 50 years), at distances 64 and 120m from the assumed site, has been examined and shown in figure 5. For both scenarios, $M_w \sim 7.7$, 645 years and $M_w \sim 7.7$, 645 years, the results are shown in Figures 5 a and b.

Concerning a part of the North Tabriz fault that passes through the 15th district of Tabriz city, estimating the probabilistic displacement in this area is of great importance, and predicting the areas with a higher level of surface rupture hazard is an important matter.

Considering a cross-section with a length of 2 km from the North Tabriz fault according to Figures (6, 7, and 8), the possible two-dimensional displacements for the North Tabriz fault have been estimated. To estimate the probabilistic displacement, two scenarios ($M_w \sim 7.7$, 645 years) and ($M_w \sim 7.3$, 300 years) were considered. Figure (6) shows the probabilistic displacement of the two mentioned scenarios for the 5% in 50 years. The probabilistic displacements for the 4.5 and 7.1m displacements for the first scenario are shown in Figures 6a and 6b, respectively. For the second scenario, those results are shown in Figures 6c and 6d.

For the second scenario, the probabilistic displacement values have a higher level of hazard that can be seen at greater distances from the assumed sites. The probabilistic displacement of the two scenarios for the 5% in 475 and 2475 years are shown in Figures 7 and 8, respectively. The values of displacement perpendicular to the assumed site and the amount of probability hazard in the area were investigated and illustrated in Figure (9), and the two scenarios ($M_w \sim 7.7$, 645 years) and ($M_w \sim 7.3$, 300 years) were compared. According to Figure 9a for 5% in 50 years, the scenario ($M_w \sim 7.3$, 300 years) has a higher level of hazard and can be considered the worst-case scenario. The numerical value of the displacement is obtained equally in the two displacement cases (4.5 and 7.1m). The first scenario, given that it has a larger magnitude than the second scenario ($\Delta m = 0.4$), but due to the higher return period, has a lower level of risk than the second scenario. In the case of 5% in 475 years and 2475 years, according to Figures (9b and 9c), unlike the case of 50 years, the first scenario has a higher level of hazard and is more important, and can be considered as the worst-case scenario.

5 Conclusion

Assuming the North Tabriz fault as a simple trace with a strike-slip focal mechanism, and considering two scenarios (Mw~7.7, 645yrs), and (Mw~7.3, 300yrs) and a fault section with a length of 50 - 60 km, the probabilistic displacement of the North Tabriz fault was estimated. Furthermore, considering the reported approach by Petersen (2011), the probabilistic displacements for an exceedance rate of 5% in 50, 475, and 2475 years for the principal probabilistic displacements (on fault) of the North Tabriz fault have been explored. The obtained results in this study can be summarized as follows.

- 1- We considered two scenarios according to possible displacements, return periods, and magnitudes which are reported in paleoseismic studies of the North Tabriz fault.
- 2- In the first scenario, possible displacement, return period and magnitude were selected between zero to 4.5; 645 years and Mw~7.7, respectively. In the second scenario, possible displacement, return period and magnitude were selected between zero to 7.1, 300 years, and Mw~7.3, respectively.
- 3- For both above-mentioned scenarios, the probabilistic displacements for the rate of exceedance 5% in 50, 475, and 2475 years for the principle possible displacements (on fault) of the North Tabriz fault have been estimated. For the first and second scenarios, the maximum probabilistic displacement of the North Tabriz fault at a rate of 5% in 50 years is estimated to be 186 and 230 cm.
- 4- Maximum displacements for 5% exceedance in 475 years and 2475 years in both return periods of 645 and 300 years are estimated at 469 and 655cm.
- 5- In this study, the probability displacement values of the North Tabriz fault have been obtained without considering the dip, depth, and rake of the fault, which has caused the same displacement values in the north and south plane of the fault. In future studies, it is possible to investigate the geometric properties of the source producing surface rupture and reduce the recognition uncertainty in the method of probabilistic fault displacement hazard analysis.
- 6- The lack of large instrumental earthquakes in northwestern Iran leads to more significant epistemic uncertainty in the obtained values. Due to the passing of the North Tabriz fault through the residential area of Tabriz and destructive historical earthquakes, it is crucial to estimate the possible future displacements of this fault.

Conflicts of interests

The authors declare that they have no known competing financial interests or personal relationships that could have appeared to influence the work reported in this paper.

References

Ambraseys, N.N., and Melville, C.P.: A History of Persian Earthquakes, Cambridge University Press, England, 236, 1982.

336 Barka, A.: the 17 August 1999 Izmit Earthquake, *Science.*, 285, 5435, 1858–1859,
 337 doi:10.1126/science.285.5435.1858, 1999.

338 Baize, S., Nurminen, F., Dawson, T., Takao, M., Azuma, T., Boncio, P., Marti, E.: A Worldwide and
 339 Unified Database of Surface Ruptures (SURE) for Fault Displacement Hazard Analyses, *Bull. Seismol. Soc. Am.*,
 340 499-520, <https://doi.org/10.1785/0220190144>, 2019.

341 Berberian, M.: Patterns of historical earthquake rupture on the Iranian plateau. In *Developments in Earth*
 342 *Surface Processes*, 17, <https://doi.org/10.1016/B978-0-444-63292-0.00016-8>, 2014.

343 Berberian, M., & Yeats, R. S.: Patterns of historical earthquake rupture in the Iranian Plateau, *Bull.*
 344 *Seismol. Soc. Am.*, 89, 1, 120-139, 1999.

345 Berberian, M.: Seismic Sources of the Transcaucasian Historical Earthquakes, *Nato. Asi. 2.*, 233–311.
 346 https://doi.org/10.1007/978-94-011-5464-2_13, 1997.

347 Berberian, M., and Arshadi, S.: On the evidence of the youngest activity of the North Tabriz Fault and the
 348 seismicity of Tabriz city, *Geol. Surv. Iran Rep.*, 39, 397–418, 1976.

349 Biasi, G. P., and Weldon, R. J.: Estimating surface rupture length and magnitude of paleoearthquakes from
 350 point measurements of rupture displacement, *Bull. Seismol. Soc. Am.*, 96, 1612–1623, 2006.

351 Bouchon, M., Bouin, M. P., Karabulut, H., Toksöz, M. N., Dietrich, M., Rosakis, A. J.: How Fast is
 352 Rupture during an Earthquake? New Insights from the 1999 Turkey Earthquakes, *Geophys. Res. Lett.*, 28, 14, 2723–
 353 2726, 2001.

354 Comfort, L.: Self-Organization in Disaster Response: The Great Hanshin Earthquake of January 17, 1995,
 355 *Nat. Hazards.*, 12, 1995.

356 Coppersmith, K. J., & Youngs, R. R.: Data needs for probabilistic fault displacement hazard analysis, *J.*
 357 *Geodyn.*, 29, 329–343, [https://doi.org/10.1016/S0264-3707\(99\)00047-2](https://doi.org/10.1016/S0264-3707(99)00047-2), 2000.

358 Cornell, C. A.: Engineering seismic risk analysis, *Bull. Seismol. Soc. Am.*, 58, 5, 1583–1606,
 359 <https://doi.org/10.1785/BSSA0580051583>, 1968.

360 Djamour, Y., Vernant, P., Nankali, H. R., Tavakoli, F.: NW Iran-eastern Turkey present-day kinematics:
 361 Results from the Iranian permanent GPS network, *Earth. Planet. Sc. Lett.*, 307, 1–2, 27–34,
 362 <https://doi.org/10.1016/j.epsl.2011.04.029>, 2011.

363 Ghassemi, M. R.: Surface ruptures of the Iranian earthquakes 1900-2014: Insights for earthquake fault
 364 rupture hazards and empirical relationships, *Earth-Sci. Rev.*, 156, 1–13,
 365 <https://doi.org/10.1016/j.earscirev.2016.03.001>, 2016.

366 Hemphill-Haley, M. A., and Weldon II R. J.: Estimating prehistoric earthquake magnitude from point
 367 measurements of surface rupture, *Bull. Seismol. Soc. Am.*, 89, 1264–1279,
 368 <https://doi.org/10.1785/BSSA0890051264>, 1999.

369 Hessami, K., Pantosti, D., Tabassi, H., Shabanian, E., Abbassi, M. R., Feghhi, K., & Solaymani, S.:
 370 Paleoearthquakes and slip rates of the North Tabriz Fault, NW Iran: Preliminary results, *Ann. Geophys-Italy.*, 46, 5,
 371 903–916, <https://doi.org/10.4401/ag-3461>, 2003.

372 Jennings, P. C.: Engineering features of the San Fernando earthquake of February 9, 1971, California
 373 Institute of Technology, (Unpublished), <https://resolver.caltech.edu/CaltechEERL:1971.EERL-71-02>, 1971.

374 Koketsu, K., Yoshida, Sh., Higashihara, H.: A fault model of the 1995 Kobe earthquake derived from the
 375 GPS data on the Akashi Kaikyo Bridge and other datasets, *Earth. Planets. Sp.*, 50, 10, 803,
 376 <https://doi.org/10.1186/BF03352173>, 1998.

377 Lee J. C., Chu H. T., Angelier, J., Chan Y.C., Hu J.C., Lu C.Y., Rau R.J.: Geometry and structure of
378 northern surface ruptures of the 1999 Mw=7.6 Chi-Chi Taiwan earthquake: influence from inherited fold belt
379 structures: *J. Struct. Geol.*, 24, 1, 173–192, [https://doi.org/10.1016/S0191-8141\(01\)00056-6](https://doi.org/10.1016/S0191-8141(01)00056-6), 2002.

380 Masson, F., Djamour, Y., Van Gorp, S., Chéry, J., Tatar, M., Tavakoli, F., Vernant, P.: Extension in NW
381 Iran driven by the motion of the South Caspian Basin, *Earth. Planet. Sc. Lett.*, 252, 1–2, 180–188,
382 <https://doi.org/10.1016/j.epsl.2006.09.038>, 2006.

383 Mirzaei, N., Gao, M. and Chen, Y. T.: Seismic source regionalization for seismic zoning of Iran: Major
384 Seismotectonic provinces, *J. Earthquake. Pred. Res.*, 7, 465–495, 1998.

385 Moss, R. E. S., & Ross, Z. E.: 2011, Probabilistic fault displacement hazard analysis for reverse faults,
386 *Bull. Seismol. Soc. Am.*, 101, 4, 1542–1553, <https://doi.org/10.1785/0120100248>, 2011.

387 Mousavi-Bafrouei, S. H., Mirzaei, N., and Shabani, E.: A declustered earthquake catalog for Iranian
388 plateau, *Ann. Geophys-Italy.*, 57, 6, <https://doi.org/10.4401/ag-6395>, 2014.

389 Paul C., Rizzo Associates, I.: Probabilistic Fault Displacement Hazard Analysis Krško East and West Sites
390 Proposed Krško 2 Nuclear Power Technical Report Probabilistic Fault Displacement Hazard Analysis Krško East
391 and West Sites Proposed Krško 2 Nuclear Power Plant, 2013.

392 Petersen, M. D., and Wesnousky, S. G.: Fault slip rates and earthquake histories for active faults in
393 southern California, *Bull. Seismol. Soc. Am.*, 84, 1608–1649, <https://doi.org/10.1785/BSSA0840051608>, 1994.

394 Petersen, M. D., Dawson, T. E., Chen, R., Cao, T., Wills, C. J., Schwartz, D. P., & Frankel, A. D.: Fault
395 displacement hazard for strike-slip faults, *Bull. Seismol. Soc. Am.*, 101, 2, 805–825,
396 <https://doi.org/10.1785/0120100035>, 2011.

397 Ram, T. D., & Wang, G.: Probabilistic seismic hazard analysis in Nepal: *Earthq. Eng. Eng. Vib.*, 12, 4,
398 577–586, <https://doi.org/10.1007/s11803-013-0191-z>, 2013.

399 Rui, Ch., Petersen, M. D.: Improved Implementation of Rupture Location Uncertainty in Fault
400 Displacement Hazard Assessment, *Bull. Seismol. Soc. Am.*, 109, 5, 2132–2137.
401 <https://doi.org/10.1785/0120180305>, 2019.

402 Shahvar, M. P., Zare, M., and Castellaro, S.: A unified seismic catalog for the Iranian plateau (1900–
403 2011), *Seismol. Res. Lett.*, 84, 233–249, 2013.

404 Stepp, J. C., Wong, I., Whitney, J., Quittmeyer, R., Abrahamson, N., Toro, G., Sullivan, T.: Probabilistic
405 seismic hazard analyses for ground motions and fault displacement at Yucca Mountain, Nevada: *Earthq. Spectra.*,
406 17, 1, 113–151. <https://doi.org/10.1193/1.1586169>, 2001.

407 Toksöz, M. N., ARPAT, E., & ŞARO&GLU, F. U. A. T.: The East Anatolian earthquake of 24 November
408 1976, *Nature.*, 270(5636), 423–425, <https://doi.org/10.1038/270423b0>, 1977.

409 Wells, D. L., & Coppersmith, K. J.: New Empirical Relationships among Magnitude, Rupture Length,
410 Rupture Width, Rupture Area, and Surface Displacement, *Bull. Seismol. Soc. Am.*, 84, 4, 974–1002,
411 <https://doi.org/10.1785/BSSA0840040974>, 1994.

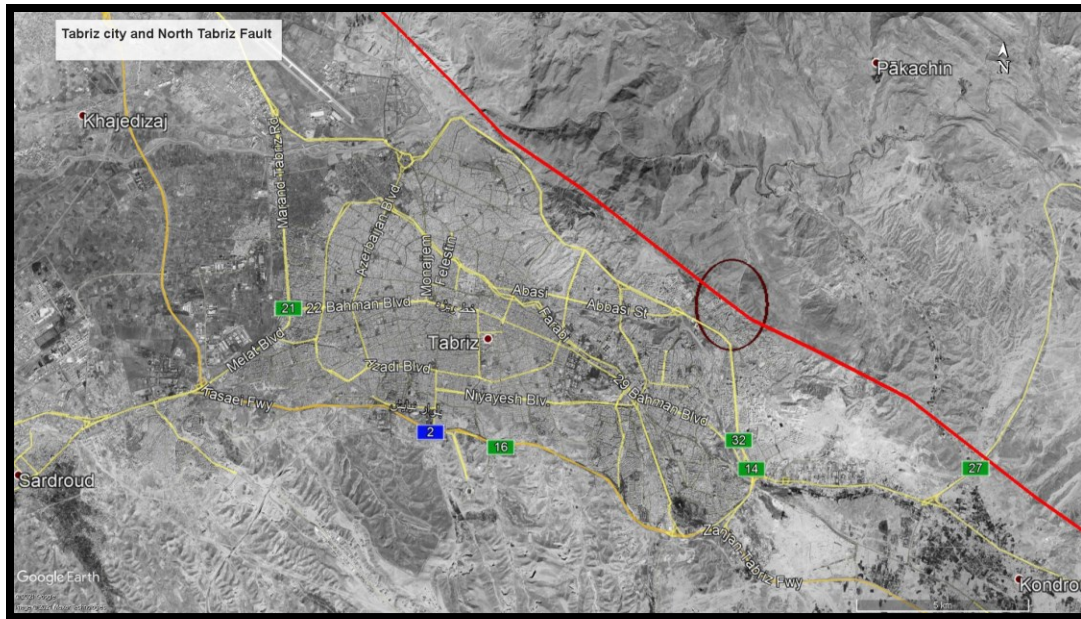
412 Wells, D. L., & Kulkarni, V. S.: Probabilistic fault displacement hazard analysis - Sensitivity analyses and
413 recommended practices for developing design fault displacements, NCEE 2014 - 10th U.S. National Conference on
414 Earthquake Engineering: Frontiers of Earthquake Engineering, October 2014, <https://doi.org/10.4231/D3599Z26K>,
415 2014.

416 Wesnousky, S. G.: Displacement and geometrical characteristics of earthquake surface ruptures: Issues and
417 implications for seismic-hazard analysis and the process of earthquake rupture, *Bull. Seismol. Soc. Am.*, 98, 4,
418 1609–1632. <https://doi.org/10.1785/0120070111>, 2008.

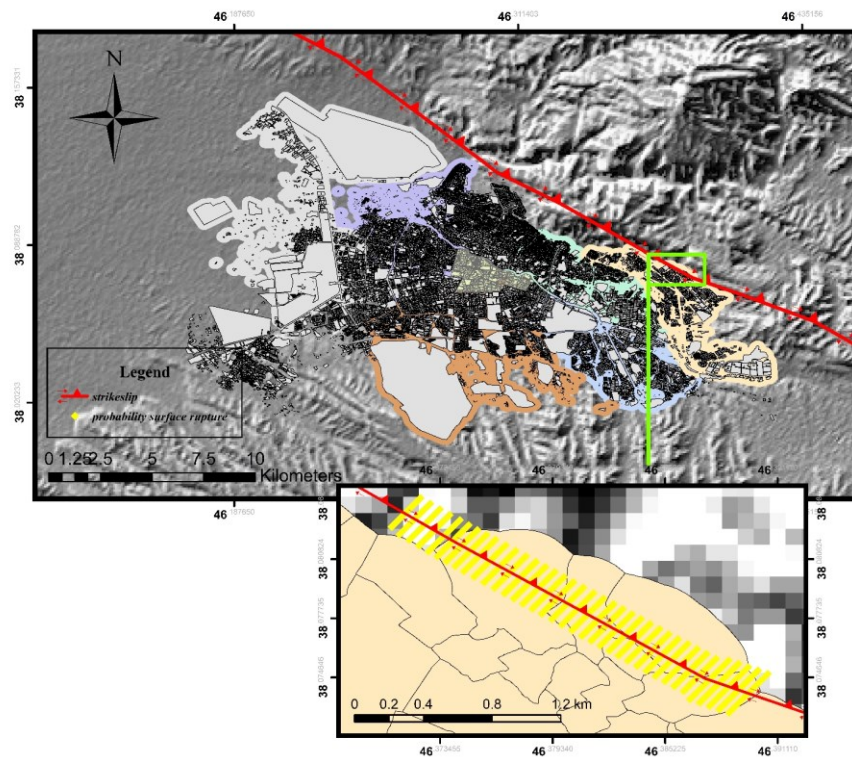
Young, C. J., Lay, T., & Lynnes, C. S.: Rupture of the 4 February 1976 Guatemalan earthquake: Bull. Seismol. Soc. Am., 79, 3, 670-689, <https://doi.org/10.1785/BSSA0790030670>, 1989.

Youngs, R. R., Arabasz, W. J., Anderson, R. E., Ramelli, A. R., Ake, J. P., Slemmons, D. B., Toro, G. R.: A methodology for probabilistic fault displacement hazard analysis (PFDHA), Earthq. Spectra., 19, 1, 191–219. <https://doi.org/10.1193/1.1542891>, 2003.

List of figures:



(a)



(b)

Figure 1. North Tabriz Fault and Tabriz city (a), Part of the North Tabriz fault considered in this study, and perpendicular profiles (b). Figure a and b are generated using Google Earth with Digital Globe imagery (© Google Earth 2021).

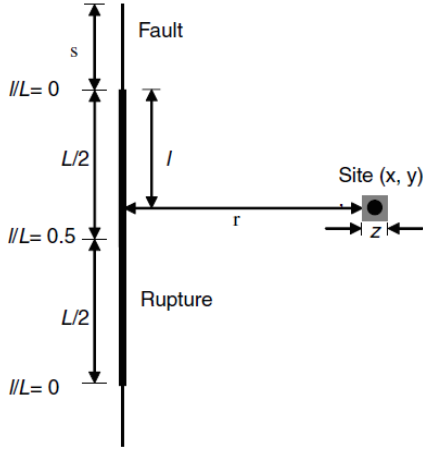


Figure 2. Definition of the variables used in fault rupture analysis: x and y Site coordinates, z Dimensions of the area intended to calculate the probability of fault rupture at the site (for example, dimensions of the building foundation), r: the distance from the site to the fault trace, ratio l/L : the distance from the fault so that l is the measured distance from the nearest point on the rupture to the nearest end of the rupture, L : the total length of the rupture and s : the distance from the end of the rupture to the end of the fault (Petersen et al., 2011).

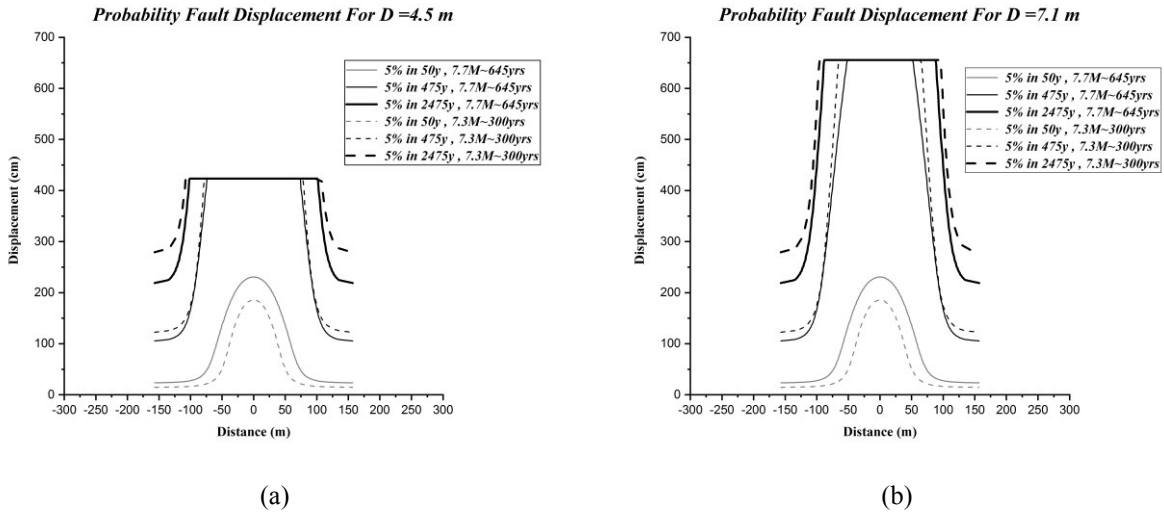
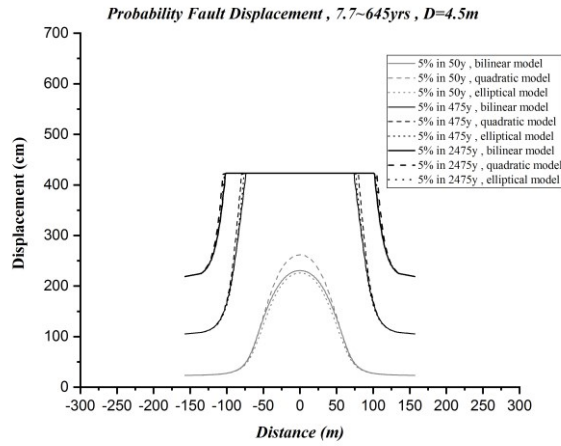
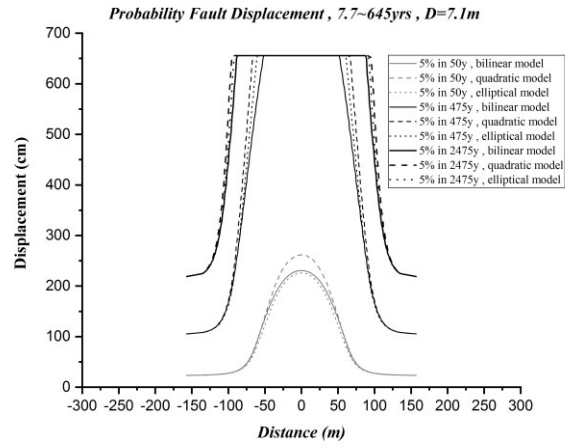


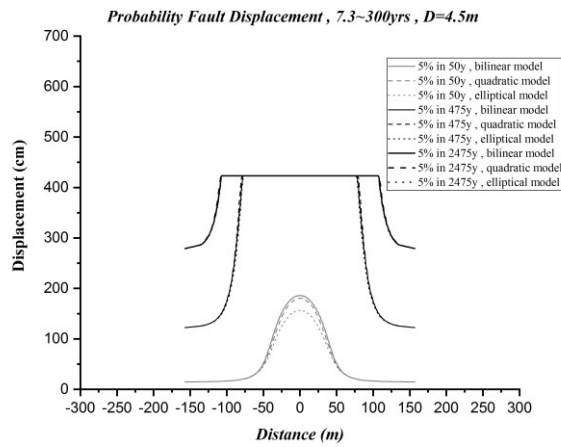
Figure 3. Comparison of probability displacement, 5% exceedance rate in 50, 475, and 2475 years for a) $D=4.5$ m b) $D=7.1$ m



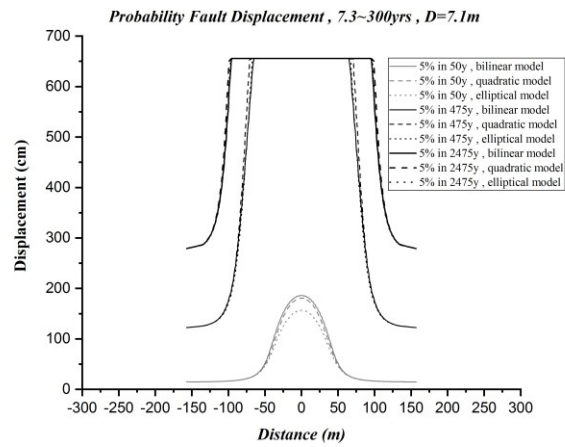
(a)



(b)

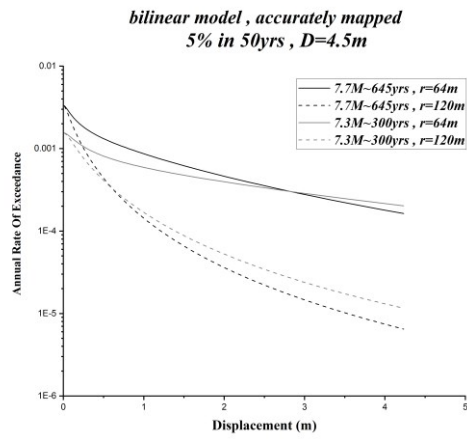


(c)

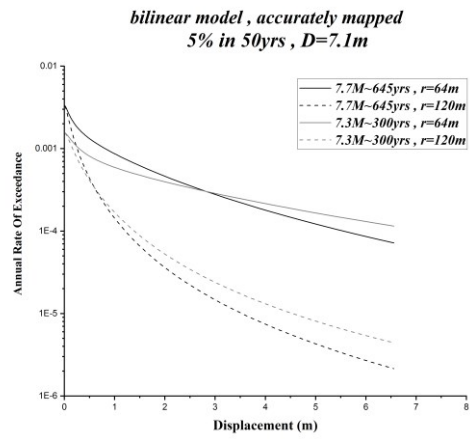


(d)

Figure 4. Comparison of probability displacement, different fitting models for a) 645-year return period and $D=4.5$ m, b) 645-year return period and $D=7.1$ m, c) 300-year return period and 4.5 m, d) return period 300- years, and $D=7.1$ m

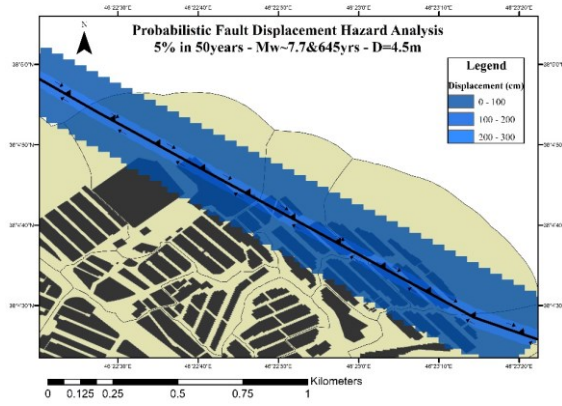


(a)

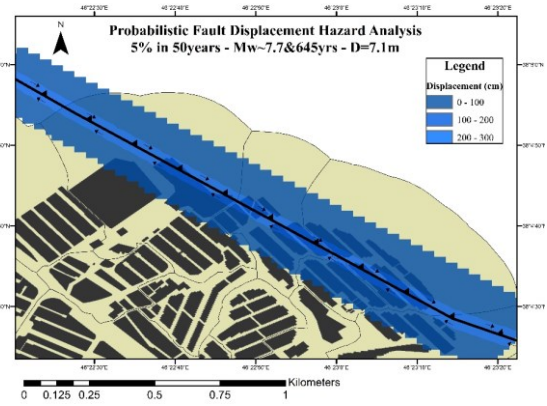


(b)

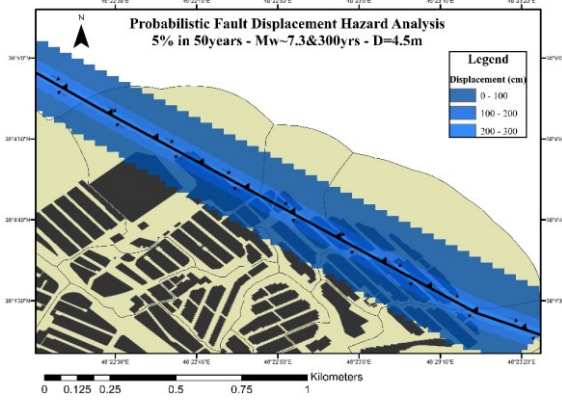
Figure 5. Comparison of the annual rate of exceedance of displacement for a) $D=4.5$ m displacement, b) $D=7.1$ m displacement



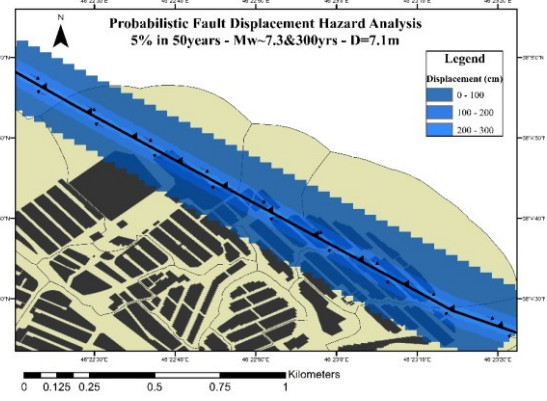
(a)



(b)



(c)



(d)

Figure 6. Probability Displacement of 5% in 50, a) Mw~7.7 and return period of 645yrs for D=4.5m, b) Mw~7.7 and return period of 645yrs for D=7.1m, c) Mw~7.3 and return period of 300yrs for D=4.5m and d) Mw~7.3 and return period of 300yrs for D=7.1m

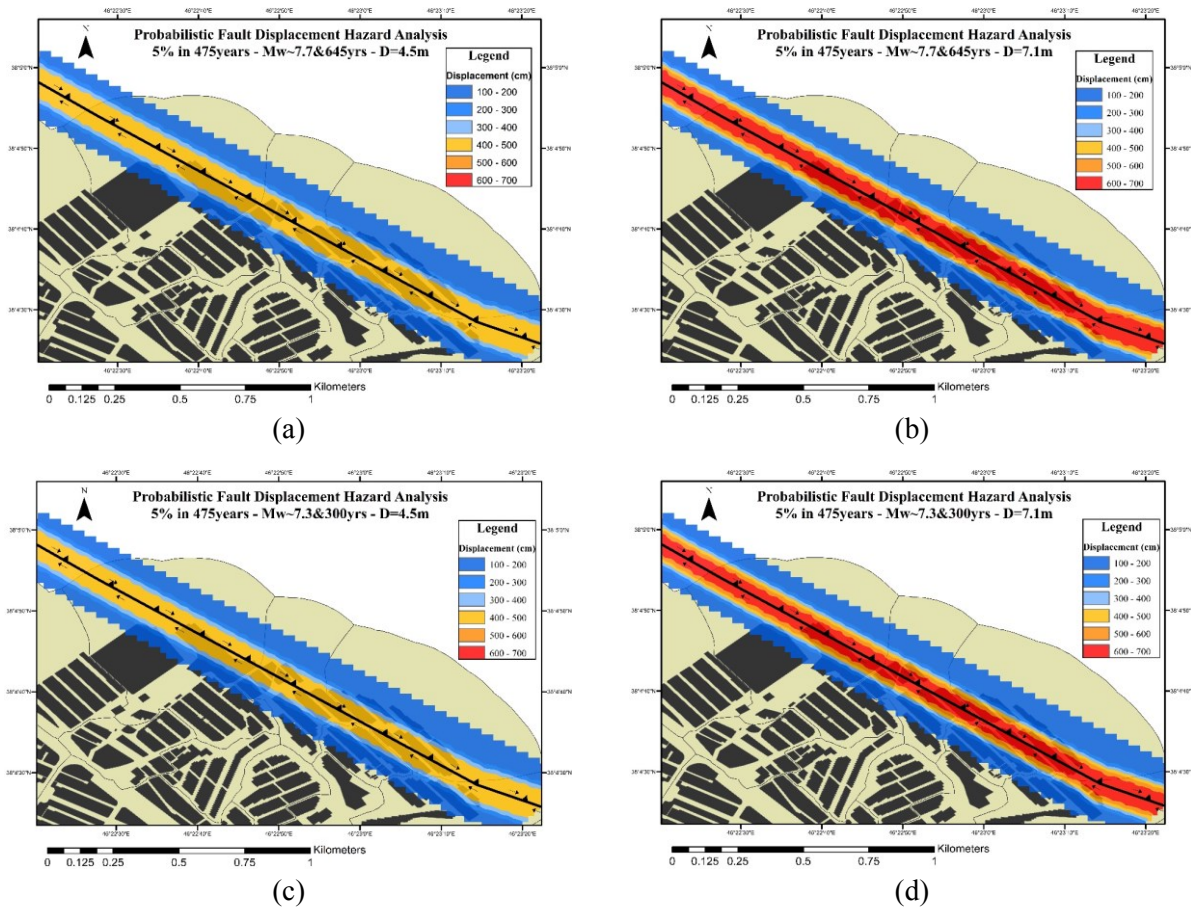
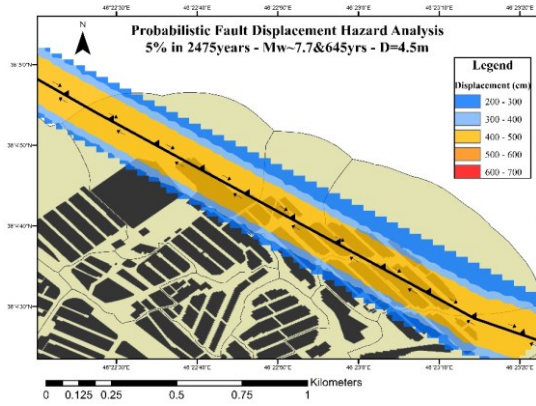
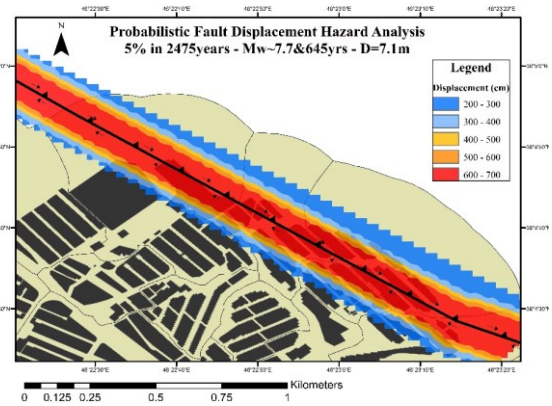


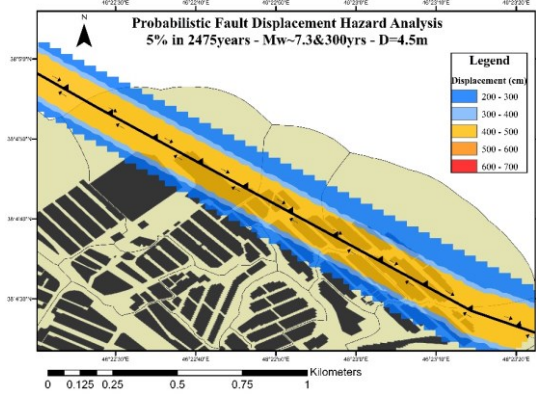
Figure 7. Probability Displacement of 5% in 475, a) Mw~7.7 and return period of 645yrs for D=4.5m, b) Mw~7.7 and return period of 645yrs for D=7.1m, c) Mw~7.3 and return period of 300yrs for D=4.5m and d) Mw~7.3 and return period of 300yrs for D=7.1m



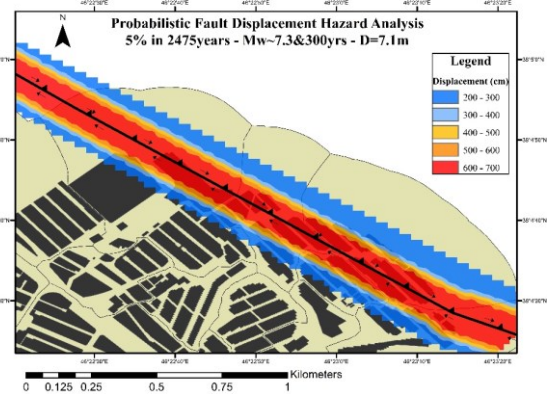
(a)



(b)



(c)



(d)

Figure 8. Probability Displacement of 5% in 2475, a) Mw~7.7 and return period of 645yrs for D=4.5m, b) Mw~7.7 and return period of 645yrs for D=7.1m, c) Mw~7.3 and return period of 300yrs for D=4.5m and d) Mw~7.3 and return period of 300yrs for D=7.1m

519 **List of Tables:**

520

521

Table 1. Probability of distributed rupture for different cell sizes (Petersen et al., 2011)

No.	Cell Size (m ²)	a(z)	b(z)	Standard Deviation(σ)
1	25×25	-1.1470	2.1046	1.2508
2	50×50	-0.9000	0.9866	1.1470
3	100×100	-1.0114	2.5572	1.0917
4	150×150	-1.0934	3.5526	1.0188
5	200×200	-1.1538	4.2342	1.0177

526

527

528

529

530

531

532

Table 2. Summary of mapping accuracy: The measured distance from the mapped fault trace to the observed surface rupture (Petersen et al., 2011)

Mapping Accuracy	Mean (m)	One-Sided Standard Deviation (m)	Two-Sided Standard Deviation on Fault (m)
ALL	30.64	43.14	52.92
Accurate	18.47	19.54	26.89
Approximate	25.15	35.89	43.82
Concealed	39.35	52.39	65.52
Inferred	45.12	56.99	72.69

533

534

535

Table 3. Different Models Used in Principal Fault Attenuation Relationships (Petersen et al., 2011)

Analysis Type	Model	Weight
Multivariate	BILINEAR $\ln(D)=1.7969M_w+8.5206(l/L)-10.2855, \sigma_{in} = 1.2906, l/L < 0.3$ $\ln(D)=1.7658M_w-7.8962, \sigma_{in} = 0.9624, l/L \geq 0.3$	0.34
	QUADRATIC $\ln(D)=1.7895M_w+14.4696(l/L)-20.1723(l/L)^2-10.54512, \sigma_{in} = 1.1346$	0.33
	ELLIPTICAL $\ln(D)=3.3041\sqrt{1-\frac{1}{0.5^2}[(l/L)-0.5]^2}+1.7927M_w-11.2192, \sigma_{in} = 1.1348$	0.33

